ASTM INTERNATIONAL

Geotechnical Testing Journal

Shad E. Hoover,[1] Whitney Greenawalt,[2] and Brian Tittmann[3]

DOI: 10.1520/GTJ20130197

Experimental and Theoretical Modeling of Expansion in Pyritic Shale

VOL. 38 / NO. 2 / MARCH 2015

Geotechnical Testing Journal

doi:10.1520/GTJ20130197 / Vol. 38 / No. 2 / March 2015 / available online at www.astm.org

Shad E. Hoover,[1] Whitney Greenawalt,[2] and Brian Tittmann[3]

Experimental and Theoretical Modeling of Expansion in Pyritic Shale

Reference

Hoover, Shad E., Greenawalt, Whitney, and Tittmann, Brian, "Experimental and Theoretical Modeling of Expansion in Pyritic Shale," *Geotechnical Testing Journal*, Vol. 38, No. 2, 2015, pp. 166–178, doi:10.1520/GTJ20130197. ISSN 0149-6115

ABSTRACT

Expansive pyritic shales are found in black carbonaceous shales throughout the United States as well as in other countries, including Ireland, England, Norway, Canada, and Sweden. Expansion occurs when the pyrite, which occurs either as finely disseminated syngenetic framboids, macroscopic crystals, or diagenetic replacement fossils, oxidizes to form sulfuric acid. Various hydrous sulfates could precipitate in the complex geochemical environment; however, gypsum typically precipitates as the sulfuric acid reacts with the calcareous (calcium carbonate) component of the shale. This paper explores kinetic and passive attempts at measuring the expansion of the shale and introduces a hybrid experimental testing procedure that uses hydrogen peroxide to initiate the expansion process. The normalized expansion (h/H) for the non-intact shale and intact shale core were 0.0008 and 0.0033, respectively, after 84 days. Expansion rates of 3.5 mm/year/m and 1.43 mm/year/m were calculated for the non-intact shale and intact shale core samples, respectively. A theoretical expansion model is developed that uses stoichiometric calculations to determine gypsum volume and discontinuity infilling theory to determine maximum total expansion. Input variables include shale type (intact bedrock, poorly-graded fragments, well-graded fragments), % pyritic shale ($\%S_2$), height of the expansion zone, and surcharge pressure. The theoretical model is used to predict maximum height of expansion and time to maximum expansion for the experiments studied and developed.

Keywords

expansive modeling, pyritic shale, heave prediction

Manuscript received December 6, 2013; accepted for publication December 8, 2014; published online January 19, 2015.

[1] Principal, CMT Laboratories, Inc., 2701 Carolean Industrial Drive, State College, PA 16801, e-mail: shoover@cmtlabsinc.com

[2] Project Engineer, CMT Laboratories, Inc., 2701 Carolean Industrial Drive, State College, PA 16801, e-mail: wgreenawalt@cmtlabsinc.com

[3] Project Engineer, CMT Laboratories, Inc., 2701 Carolean Industrial Drive, State College, PA 16801, e-mail: btittmann@cmtlabsinc.com

Introduction

Structural damage to buildings and other civil infrastructure by expansive pyritic shale is becoming increasingly prevalent as construction continues to expand into undeveloped areas and as engineering knowledge of the damaging effects of building on or with this material remains inadequate. Case histories involving expansive pyritic shales are well documented; specifically, areas of the United States include Tennessee (Long and Williams 1990), Virginia (Freeman 2003), Ohio (Anonymous 1960), West Virginia (Dubbe et al. 1984), Pennsylvania (Hoover 2004), and Missouri and Kansas (Coveney and Parizek 1977). The expansive pyritic shale problem is also found in Ireland (McCabe et al. 2012), England (Hawkins and Pinches 1987), Norway (Moum and Rosenquist 1959), Canada (Tanguay et al. 1999; Penner and Eden 1972), and Sweden (Jangdal 1971). Heaving of the infamous Marcellus Shale formation in Lewisburg, PA has resulted in the need for underpinning and significant structural repairs to the Evangelical Hospital (Hoover and Pease 2007) and use of the Reedsville Shale as fill material has damaged numerous structures throughout Centre County, PA.

The geochemical process responsible for expansion of pyritic shales is complex. Attempts were made to model the process using PHREEQC (Hoover and Lehmann 2009), which is a hydrogeochemical transport modeling program. The theory behind the geochemistry requires the presence of pyrite (FeS_2), calcite ($CaCO_3$), oxygen (O_2), and water (H_2O). Simply described, when the *available* pyrite within the shale reacts with water and oxygen, the result is the production of sulfuric acid (H_2SO_4). The sulfuric acid reacts with the *available* calcite resulting in the precipitation of gypsum ($CaSO_4 \bullet H_2O$). The stoichiometry is described in further detail in the theoretical modeling portion of this paper. Other factors, such as temperature, pyrite morphology, *p*H, and microbial oxidation, can influence the reaction rates and amount of gypsum produced. The oxidation of pyrite produces hydrous sulfates, such as melanterite ($FeSO_4 \bullet 7H_2O$) and halotrichite ($FeAl_2(SO_4)_4 \bullet 22H_2O$), as well as base exchange products such as ochre (FeO(OH)) and jarosite ($KFe_3(SO_4)_2(OH)_6$. The negative environmental impacts of pyrite oxidation result in acid rock drainage (ARD) and acid mine drainage (AMD). The geochemistry of pyrite oxidation and environmental mitigation efforts are well established but far from perfected (Brady et al. 1998).

The greatest barrier to truly understanding the complexity of the geochemistry of pyrite oxidation is understanding how the pyrite becomes available for reaction with a moist or humid *micro*environment. Crystalline ("fools gold") or macroscopic pyrite "locked" away within a strong rock, such as limestone, will not be sufficiently available to react to a humid environment. The larger surface area of crystalline and certainly macroscopic pyrite, e.g., replacement fossils or burrows, significantly reduces the reaction rate to a geologic timescale. Pyrite within black carbonaceous shales typically comes in the form of framboidal shaped microcrystals measuring between 0.1 and 10 μms in diameter (Schieber and Baird 2001). **Figure 1** is a cross-sectional image of Marcellus Shale under a scanning electron microscope (SEM) that shows distribution of pyrite microcrystals into framboidal clusters. Increased surface area associated with pyrite microcrystals and cluster results in high reactivity rates that correspond well with expansion rates beneath damaged structures (Rimstidt and Newcomb 1993). The reactivity of macroscopic pyrite in shales is similarly restrictive; however, the parent rock is much weaker and the presence of discontinuities and stress relief fracturing make the pyrite more available for reaction. The reaction rate of macroscopic pyrite will be increased in the right microenvironment wherein the *p*H drops to a point where oxidizing ferric iron (Fe^{3+}) and/or microbial oxidation (acidithiobacillus ferrooxidans) thrive (Jaynes et al. 1984a,1984b).

The current state-of-practice to determine the potential for expansion is to (a) verify that the rock is shale or shaly in nature and (b) determine the amount of pyritic sulfur by using the ASTM–EPA method outlined in the Pennsylvania DER manual. Using either the LECO titration or infrared technique can determine the amount of pyritic sulfur. Various resources suggest that 0.1 % pyritic sulfur by weight is sufficient to define a material as "potentially" expansive (Dougherty and Barsotti 1972); however, industry wide expansion testing methodologies are not well coordinated and predictive heave calculations simply do not exist. This paper attempts to further the experimental expansion testing database and enter into the realm of theoretical predictive heave calculations.

Experimental Expansion Testing

Three approaches to expansion testing will be studied. The first experiment can be considered a kinetic approach to inducing

FIG. 1 Backscatter images of framboidal clusters of pyrite microcrystals.

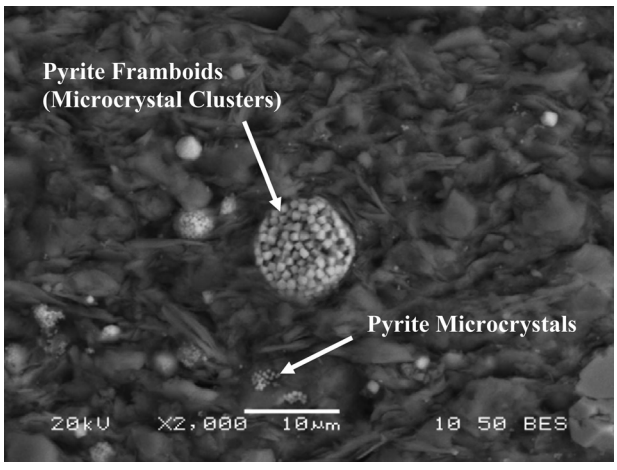

expansion in pyritic shales. Although not successful in producing measureable expansion, the chemistry of the oxidized solution produced data useful for the understanding the rate of oxidation of the shale. The second experiment can be considered a passive approach to studying expansion in pyritic shales or mudstones that have already begun to swell. The passive experiment was very successful in measuring expansion over a relatively long period of time. The third experiment can be considered a hybrid of the first two; specifically, hydrogen peroxide was utilized to accelerate the oxidation process at the beginning and the expansion permitted to proceed under passive conditions.

KINETIC OXIDATION COLUMN EXPERIMENT

Bulk shale samples from the Marcellus Formation were taken from an undisclosed site located near Washingtonville, PA. The black shale contained pyrite replacement fossils and possible vein-filling pyrite deposits. In addition, samples near the surface

FIG. 2

(*a*) Schematic diagram and (*b*) photograph of actual setup for swell experiments using kinetic oxidation techniques (for scale note that each cylinder is approximately 3 in. in diameter).

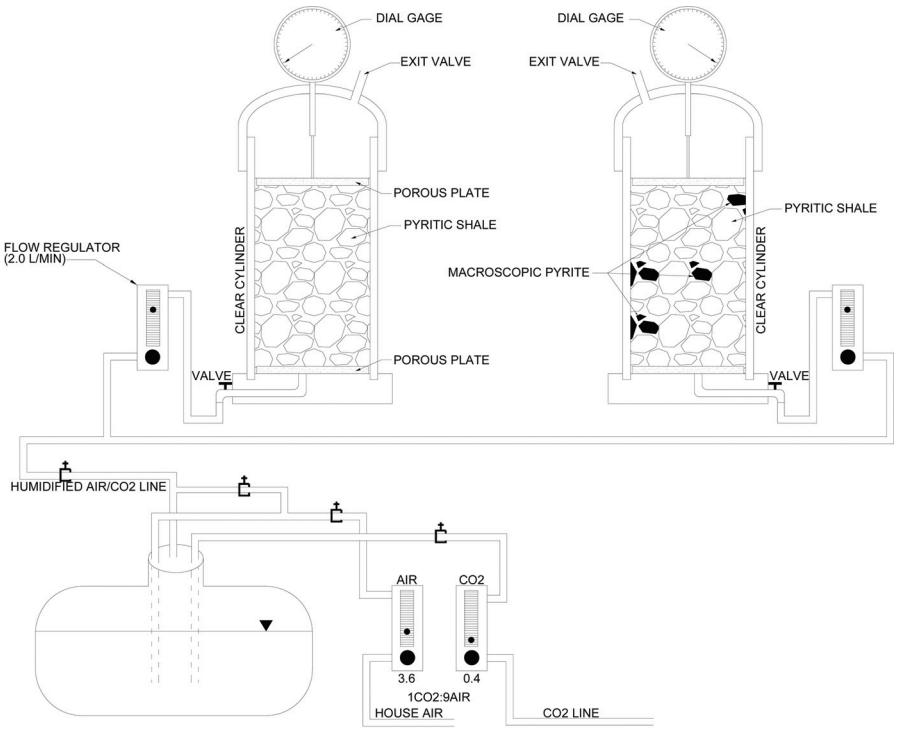

a)

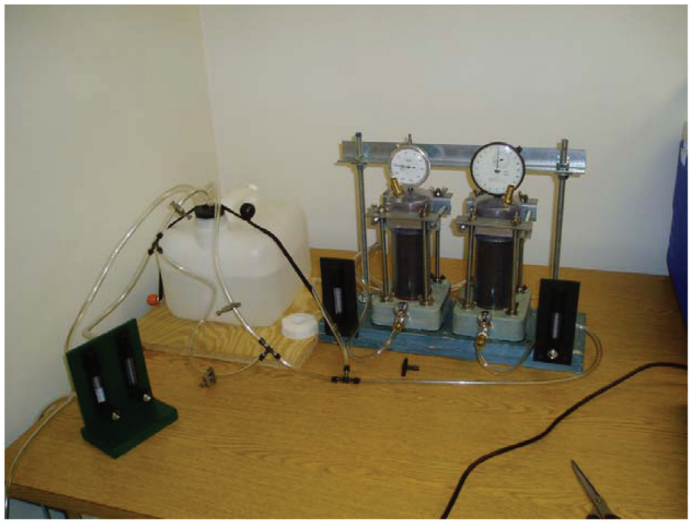

b)

of the site contained evidence of swelling due to the presence of various hydrous sulfates, such as gypsum and jarosite.

Two separate kinetic columns were prepared with crushed shale fragments, which were fairly well-graded with all particles passing the 12.70 mm sieve and less than 1 % passing the 0.850 mm sieve. The first column contained no visible or macroscopic pyrite and had pyritic sulfur (S_2) and calcium carbonate ($CaCO_3$) values of 1.57 and 5.7 % by weight, respectively. The second column contained macroscopic pyrite and had S_2 and $CaCO_3$ values of 2.49 and 5.7 % by weight, respectively. A schematic diagram and a photograph of the setup for the swell experiments using kinetic oxidation techniques are shown in **Figs. 2(*a*)** and **2(*b*)**, respectively.

Humidified air with 10 % carbon dioxide (CO_2) was introduced into each column for six days to allow for oxidation of pyrite. A 9 + 1 ratio by volume/volume of air to CO_2 was established to allow for a maximum test period of approximately 90 days. One cycle consisted of establishing a flow rate of 2.0 l/min and maintained for each column for six days followed by a 24-h period of pumping dry air through the samples to encourage precipitation of hydrous sulfates. This cycle was continued for approximately 20 days followed by a period of inundation with water. The air/CO_2 mixture was pumped into the inundated samples for 24 h and the effluent was sampled for sulfate anion and *p*H testing. The effluent was taken after the 24 h inundation period (see **Fig. 3** for frequency).

No swelling of the shale fragments was measured in the dial gauges during the kinetic experiment; however, the sulfate anion concentration and *p*H of the effluent were taken after the various inundation periods and are presented in **Figs. 3** and **4**, respectively. These results were used to analyze the progression of pyrite oxidation and the changes to the bulk chemistry of the solution.

There is estimated 2 % pyritic sulfur content in the shale particles utilized for both columns and an additional 1.6 % concentrated pyritic sulfur added to column "B." Given the amount of sulfate leached and the estimated pyritic sulfur contents in each of the columns, a total of approximately 1 % of the pyritic sulfur has been oxidized during the 84 days of the experiment. There is no geochemical evidence to suggest that the added macroscopic pyrite in column B has undergone any appreciable oxidation.

PASSIVE EXPANSION TESTING

McCabe et al. (2012) presented a laboratory study of active pyritic shale, which has caused extensive damage to a structure in Ireland. Floor heave of the structure measured between 5 mm (0.2 in.) and 11 mm (0.43 in.) after a period of approximately five years. The thickness of the fill ranged between 500 mm (20 in.) and 750 mm (30 in.). Rates of expansion varied between 2.0 mm/year/m (0.0020 in./year/in) and 2.9 mm/year/m (0.0029 in./year/in). Surcharge on the shale is unknown. The

FIG. 3 Sulfate concentration of effluent in kinetic oxidation column experiment.

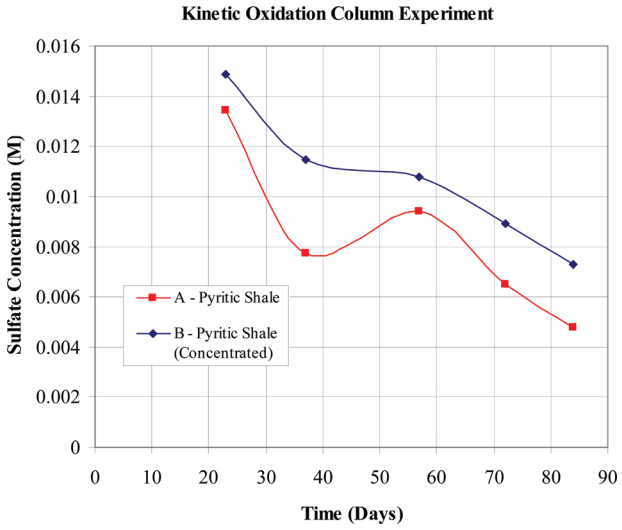

shale fragments corresponded to a poorly-graded gravel with sand and silt sized particles. Pyritic sulfur concentrations of the fill ranged between 1.87 and 2.58 %.

The fill was placed and compacted in clear plastic tubes measuring 225 mm (8.8 in.) in diameter with lengths of 500 mm (20 in.), 750 mm (30 in.) and 1000 mm (40 in.). The pipes were then placed in plastic containers filled with water to varying depths. One pipe was not placed in any water.

The passive oxidation swell experiment was conducted over a period of 175 days. Normalized expansion (h/H) varied between 0.0008 and 0.0012. Expansion rates ranged between 2.3 mm/year/m of fill (0.0023 in./year/in.) and 2.9 mm/year/m of fill (0.0029 in./year/in.), which is consistent with field

FIG. 4 *p*H of effluent in kinetic oxidation column experiment.

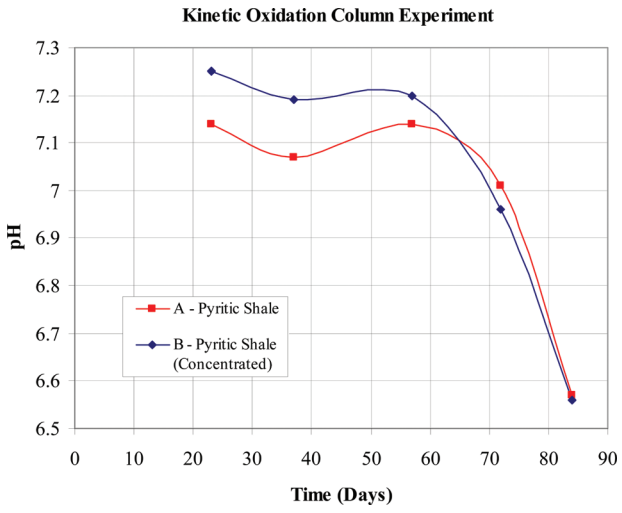

TABLE 1 Initial testing results for hydrogen peroxide expansion testing program.

Sample	Gradation	Sample Height (in.)	Void Ratio	Dry Density (lbf/ft^2)	S_2 (%)	FeS_2 (%)	$CaCO_3$ (%)	$CaCO_3$:FeS_2 Molar Ratio
A	Poorly-graded sand	7.80	0.876	89.90	2.07	3.76	9.82	3.13
B	Poorly-graded gravel	7.80	0.837	91.73	2.19	3.97	9.71	2.93
C	Well-graded gravel	8.00	0.777	94.82	2.10	3.81	9.71	3.05
D	Intact rock core	6.25	<0.10	165	1.48	2.68	15.24	6.80

measurements. The largest amount of expansion surprisingly took place in the sample that was not placed in water.

HYDROGEN PEROXIDE EXPANSION TESTING

Given the failure of the kinetic oxidation approach to expansion testing and the successes given by the passive approach offered by McCabe et al. (2012), a new oxidation methodology has been tried. McCabe et al.'s passive approach produced significant expansion, but it took a significant amount of time (175 days) for expansion to occur and it was conducted on material that already was expanding in the field. The hydrogen peroxide approach has been attempted in order to potentially provide an accelerated view into the expansive potential of pyritic shale.

Rock core samples from the Marcellus Shale Formation in Lewisburg, PA, were chosen for this experiment. The rock cores were taken from depths ranging between 6.1 and 9.1 m (20 and 30 ft) below the existing ground surface. The samples were relatively fresh showing little signs of weathering. Point load tests on the rock cores revealed an average unconfined compressive strength of 12 560 psi. Sulfur analyses were performed on the rock, which revealed S_2 concentrations ranging between 1.48 and 2.19 % by weight. Moreover, these analyses indicated that the rock contained $CaCO_3$ concentrations ranging between 9.82 and 15.24 %. The $CaCO_3$:FeS_2 molar ratio of the samples ranged between 2.93 and 6.80. Note that a 2:1 molar ratio is required in an open system in order for that system to produce the maximum amount of gypsum from pyrite oxidation (Hoover and Lehmann 2009).

Four separate samples were chosen for the expansion testing. Three samples were fractured in an LA Abrasion machine and sieved for specific gradation. The last sample consisted of an intact rock core. **Table 1** provides a description of each sample.

Each sample was placed in a Schedule 40 clear PVC pipe with a base consisting of automobile body polyester. The devices are capable of allowing the hydrogen peroxide solution to fluctuate through the shale samples. A schematic diagram and a photograph of the setup for the swell experiments using the hydrogen peroxide expansion techniques are shown in **Figs. 5(*a*)** and **5(*b*)**, respectively.

The next step in the experiment was to determine an optimal hydrogen peroxide (H_2O_2) concentration. Several shale fragments were placed in a beaker and subjected to H_2O_2 concentrations of 3, 10, and 30 %. Each concentration produce hydrous sulfate crystal precipitation upon evaporation; however, visually, it appeared that 10 % would be the optimal concentration. The 3 % solution produced trace gypsum crystal on the surface of the shale fragments. The 10 % solution produced even more crystallization; however, the 30 % solution produced a violent reaction as the solution came to a boil. **Figures 6(*a*)** and **6(*d*)** are optical images of the gypsum precipitation on the shale fragments subjected to 0 % (washed fragments for gradation preparation), 3, 10, and 30 % hydrogen peroxide, respectively.

Note the change in gypsum crystal morphology as the concentration of hydrogen peroxide increases. Oxidation with water produced a white crystal with typical "twinning." Oxidation with 3 % H_2O_2 produced a transparent crystal with similar monoclinic "twinning" as produced with water oxidation.

FIG. 5 (*a*) Schematic diagram and (*b*) photograph of actual setup for swell experiments using hydrogen peroxide oxidation techniques (for scale note that each cylinder is approximately 3 in. in diameter).

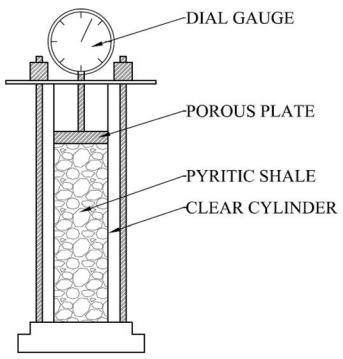

a)

b)

FIG. 6

Optical images of gypsum crystal formation at 100X for (*a*) H_2O, (*b*) 3 % H_2O_2, (*c*) 10 % H_2O_2, and (*d*) 30 % H_2O_2.

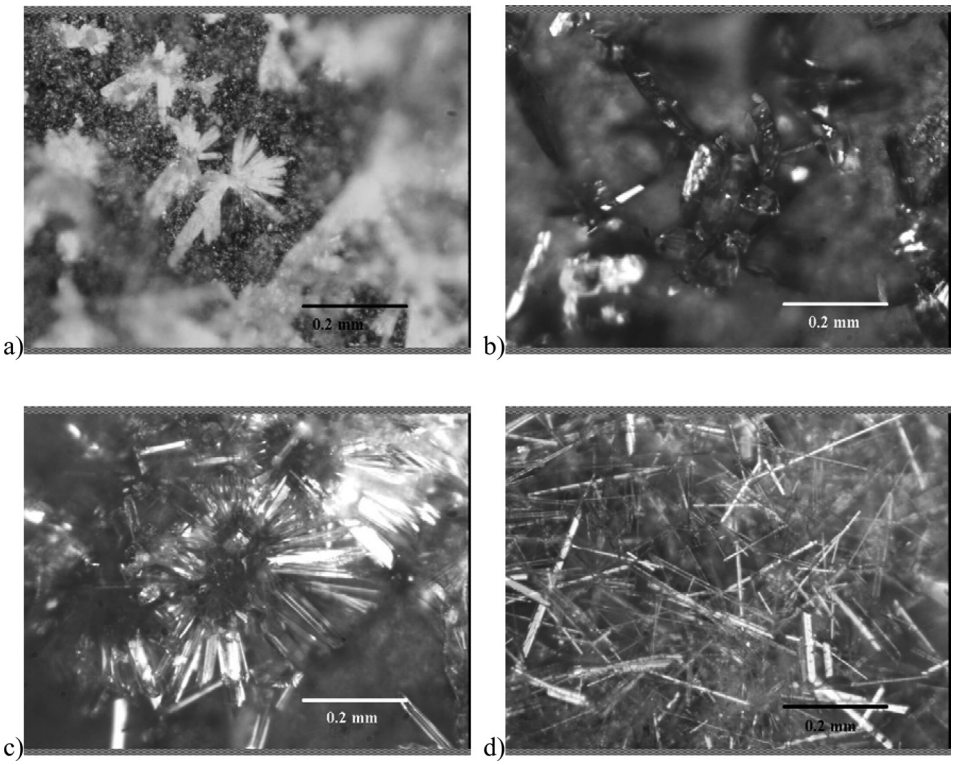

The crystal morphology changed to more elongated monoclinic crystals with a flowerlike presentation for the 10 % H_2O_2. Finally, the gypsum crystals became "needlelike" and disorganized with the 30 % H_2O_2.

Step one of the oxidation and expansion measurement process was to inundate the samples with 10 % hydrogen peroxide for 7 days. During this phase, the caps were kept closed. While measuring expansion during the first phase, the solution was drained to three-fourths of the height of the sample at day 7. Expansion measurements were taken for an additional 21 days, at which point the valves were open to allow for evaporation. After an additional 7 days of measurements and observation, the vented caps were taken completely off to allow for more exposure to the atmosphere and evaporation of the solution. From this point on, as the solution continued to evaporate, the samples began expanding at different rates. Samples B (poorly-graded gravel) and C (well-graded gravel) essentially did not exhibit any expansion, while Sample A (poorly-graded sand) began to swell as well as Sample D (rock core). The normalized expansion (h/H) for Samples A and D were 0.0008 and 0.0033, respectively, after 84 days. Expansion rates for Samples A and D were 3.53 mm/year/m (0.0035 in./year/in.) and 14.26 mm/year/m (0.0143 in./year/in.), respectively. A normalized expansion graph for the hydrogen peroxide expansion experiment is shown in **Fig. 7**.

IDENTIFYING GYPSUM USING A STAINING TECHNIQUE

The next step, now that the experimental expansion was completed, was to identify whether the gypsum forming process took place in the four samples. To accomplish this, the loose particles of the sand and gravel needed to be solidified. This was done by means of a low viscosity epoxy formed by mixing EpoHeat[4] Resin and EpoHeat Hardener. The cylinders had a vacuum system attached to their top, while a short tube was attached to their bottom. The tube was lowered into a container of the epoxy. This created a differential in pressure pushing the epoxy up through all the void spaces in the gravel and sand mixtures. This process was not performed on the rock core. Once the epoxy had fully infiltrated the sample, the vacuum was removed and the bottom spout closed off. The sample was then baked in the oven at 65°C for 90 min, thereby hardening the epoxy. The samples were then saw-cut perpendicular to the vertical axis into three or four sections. This allowed for investigation into the presence of gypsum in the interior of the sample.

A staining technique (Poole and Thomas 1975) was used to identify the existence of sulfates, e.g., gypsum, melanterite, halotrichite, etc., in the columns. This process involves immersing the sample in a mixed 10 % solution of barium chloride ($BaCl_2$) and potassium permanganate ($KMnO_4$) for 2 min.

[4]Buehler Ltd., Lake Bluff, IL.

FIG. 7 Normalized expansive graph for hydrogen peroxide swell experiment.

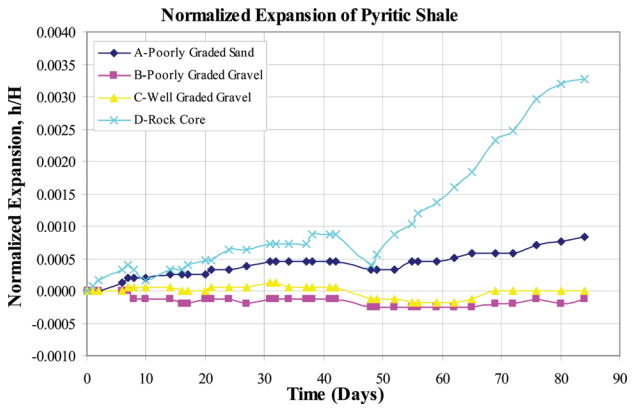

A 2 + 1 ratio by volume/volume of $BaCl_2$ to $KMnO_4$ was recommended for maximum intensity of stain color. The Barium ion reacts with the sulfate ion and precipitates with the permanganate molecules in the lattice. Thus, any sulfates formed under these conditions will be stained purple. The sample is then rinsed in a saturated solution of oxalic acid to remove excess permanganate coloration.

This staining technique was used to attempt to positively identify the presence of sulfates on the rock particles in the four samples. Two attempts were made. The first attempt was made on the horizontal faces of the columns: the saw-cut faces for the sand and gravel samples and the naturally broken faces for the rock core. No visible purple staining occurred on the saw cut faces; however, there was staining on the rock core face as shown in **Fig. 8(*a*)**. A second attempt was made on the saw cut samples. These samples were split with a chisel to create a natural break along the vertical axis of the column. These exposed jagged faces were then submitted to the staining technique. This resulted in many areas being stained purple indicating the presence of sulfates as shown in **Fig. 8(*b*)**, **8(*c*)**, and **8(*d*)**.

Experimental Expansion Testing Conclusions

KINETIC OXIDATION COLUMN EXPERIMENT

Although weathering of the shale fragments was semi-successful, the experiment failed to produce any hydrous sulfate even under SEM evaluation. The experiment failed to produce expansion for two important reasons. The first reason for failure was that the samples were not sufficiently exposed to a humid environment. The shale fragments should have been placed in a semi-saturated condition and then subjected to the air/CO_2 inflow. The second reason for failure was that flushing of the system could have easily removed any sulfate precipitation.

FIG. 8

Digital photographs of the sulfate stained purple from barium chloride and potassium permanganate solution: (*a*) rock core horizontal cross-section near the top (for scale note that the diameter of this rock core is approximately 2 in.), (*b*) Poorly graded sand vertical cross-section in the middle of the column, (*c*) poorly graded gravel vertical cross-section in the middle of the column, (*d*) well graded vertical cross-section in the middle of the column (for scale note that specimens in (*a*), (*b*), and (*c*) are all approximately 3 in. in diameter).

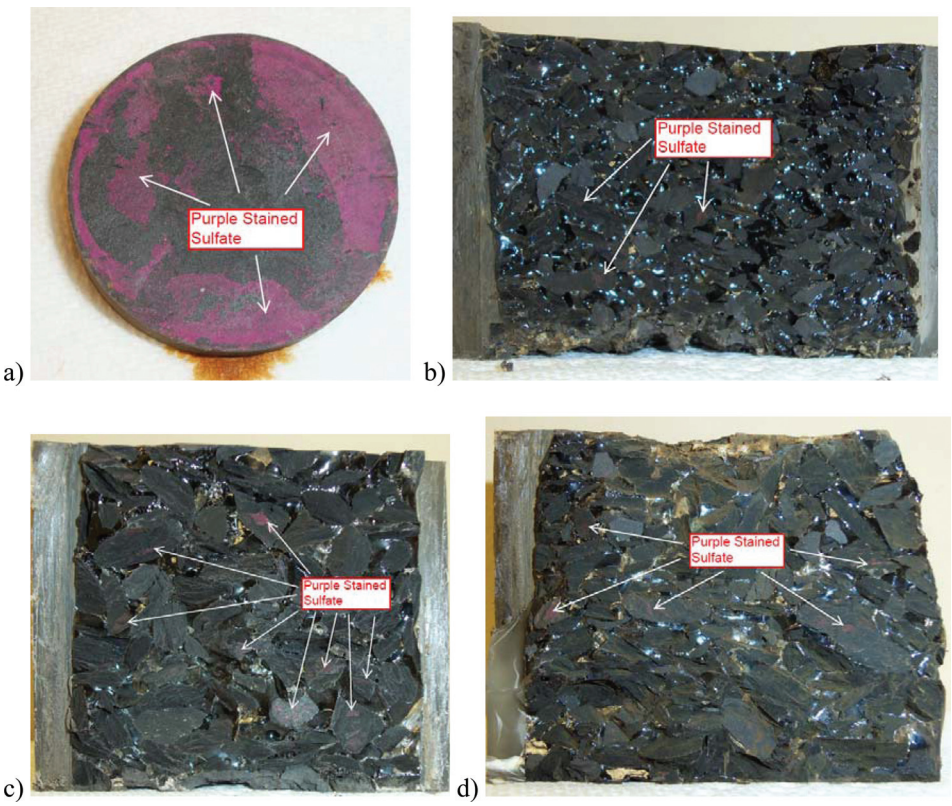

PASSIVE EXPANSION TESTING

McCabe et al.'s (2012) passive expansion test produced good results that could be utilized to predict future heave of pyritic shale fragments. Even though the mudstone was taken from a site that has a documented history of structural damage, there appeared to be sufficient pyritic sulfur to continue expansion. One of the most interesting results was that the sample with no water inundation experienced the greatest amount of heave. The reason for this may be that since the expansion process had already begun, there were sufficient microenvironmental geochemical conditions, i.e., humidity, low *p*H, possible Fe^{3+} and bacteria, to allow for hydrous sulfate precipitation. Most likely, each of the other samples would have expanded at a similar rate if they would not have been placed in a water bath.

HYDROGEN PEROXIDE EXPANSION TESTING

Expansion results were poor for Samples B (poorly-graded gravel) and C (well-graded gravel), which may be the result of poor compaction during preparation and rearrangement of particles during sulfate precipitation. Surcharging the samples may have allowed for the shale particles to expand without rearrangement. Samples A (poorly-graded sand) and D (intact rock core) experienced significant expansion in excess of the passive expansion testing experiment. Removal of the cap and lowering of the solution allowed for accelerated expansion of the samples. The rock core produced the most favorable results, which can be attributed to hydrous sulfate crystallization growth in and along the bedding planes and vertical heave perpendicular to the bedding plane.

Theoretical Expansion Model

Predicting the potential of pyritic shales to expand or swell is highly complex due to the many variables involved, and this is including, but not limited to, morphology (intact bedrock, gradation of pyritic shale fill, dip of the bedding planes, etc.), surcharge load and type (spread footing, slab-on-grade, grade beam, wall footing, drilled pier, etc.), concentration of pyritic sulfur (S_2), concentration of calcium carbonate ($CaCO_3$), modulus of elasticity of the bedrock, fill material and/or gypsum, void ratio of the fill material, thickness of the fill or thickness of the intact bedrock within the oxidation zone, Poisson's ratio of the shale and gypsum, and availability of the pyrite within the shale bedrock or shale fragments to oxidize and form sulfuric acid. The object of this model will be to simplify the expansion process as much as possible in order to determine maximum potential expansion. This model will not directly address expansion rate, which is obviously tied to oxidation rate and pyrite availability; however, possible correlations may be drawn between this model and existing experimental data.

The premise of the model is based on the observational data gathered from projects where pyritic shale resulted in structural damage. Specifically, the model is based upon the documentation of gypsum infilling within discontinuities along the bedding planes of pyritic shales fragments. Image J (National Institutes of Health) analysis of thin sections of swelled pyritic shales reveals the presence of distinct gypsum infilling in fractures within the shale. Image J is a computer program that allows for detailed analysis of thin sections, such as measuring area, mean, standard deviation, lengths, and angles. Three thin sections were taken from a single piece of shale beneath a floor slab area that has heaved approximately 7.6 cm (3.0 in.) (Hoover and Pease 2007). The shale contains abundant crystalline gypsum in very fine fractures. The thin sections consisted of the following descriptions:

S1 (PDJ): thin section perpendicular to joint
S2 (PLJ): thin section parallel to joint
S3 (PLBP): thin section parallel to bedding plane

Three sections (left–middle–right) were measured for the S1 and S2 samples to obtain the quantitative data. A total of 220 and 224 measurements were taken for samples S1 and S2, respectively. Specifically, the distance between gypsum infilling and the thickness of the gypsum infilling was measured along the entire depth of the sample at three separate cross-sections. **Figures 9(*a*)** and **9(*b*)** show examples of images utilized in the Image J analysis.

The average thickness of the gypsum infilling was measured to be 0.0482 cm (0.0190 in.) and the average distance between infilling was measured to be 0.20 cm (0.0787 in.). The extensive data gathered during this analysis revealed that gypsum growth occurred along the bedding plane either from stress relief fracturing or fracture propagation resulting from expansion of the gypsum crystals throughout other portions of the shale.

A visual representation of the expansion model is presented in **Fig. 10.** A number of assumptions have to be made in order to explain this expansion model. These key assumptions are described below:

1. The precipitation of gypsum is the only mechanism for expansion and its volume is calculated from simple stoichiometric equations involving the oxidation of pyrite, the formation of sulfuric acid, and its reaction with available calcium carbonate.
2. The gypsum forms in horizontal layers, i.e., bedding planes, perpendicular to the surcharge load. The thickness

TABLE 2 Elastic modulus and void ratio input parameters for the trial model.

	Elastic Modulus		
Shale Block Type	(ksi)	(MPa)	Void Ratio
Intact Shale	4653	32 000	0.0
Well-Graded Shale	6.94	45	0.4
Poorly-Graded Shale	3.47	23	0.8

FIG. 9 (*a*) Image S2M-5 thin section of saw cut parallel to joint and perpendicular to bedding plane (PLJ) and (*b*) image SL3-20 thin section of saw cut parallel to bedding plane (PLBP) (Hoover and Lehmann 2009).

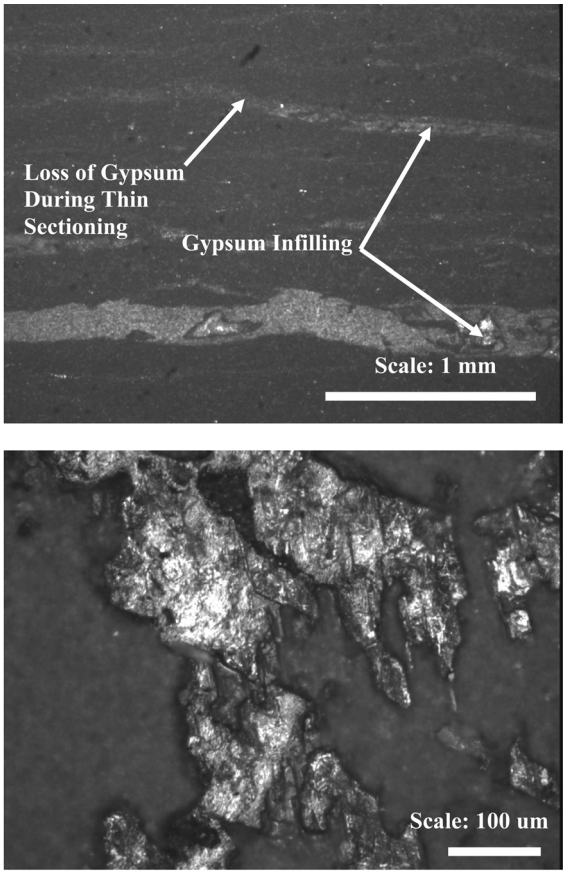

of the horizontal gypsum layers is fixed at 0.05 cm (0.02 in.) based on previously described observation data.

3. The number of layers for the gypsum infilling is a function of the volume of gypsum produced.
4. The expansion mechanism for intact shale is the same as it is for shale fragments. The model still assumes that the expansion takes place in the form of gypsum infilling; however, the amount of infilling decreases as the void ratio increases. All fragments are assumed to be oriented preferentially to allow for maximum expansion.
5. The expansion model does not account for reorientation of shale fragments or bedding planes that are not horizontal to the direction of loading.
6. Elastic compression of the pyritic shale layer assumes an infinitely and uniformly loaded surface. In addition, it is assumed that the elastic compression takes place immediately upon loading and only within the thickness specified.

The first step in the expansion prediction model is volume and weight calculations. The first input variable is the height of the potentially expansive shale stratum (H'). For natural pyritic bedrock, H' is typically equal to the distance between the bottom of the loaded area and the underlying water table or top of another non-pyritic stratum. The loaded area (A_s) is an arbitrary function of H' and can be adjusted according to field conditions as long as it is recognized that the loading is uniform and that the model does not account for size and shape factors. The total volume of the shale for the expansion model, V_T, is a function of the area, A_s, height, H', and void ratio, e_s, of the potentially expansive shale block.

$$A_S = (0.5H')^2 \tag{1}$$

$$V_T = \frac{A_s \cdot H'}{1 + e_s} \tag{2}$$

Once the total volume is determined for the expansive shale block, the mass of the pyrite and calcium carbonate can be determined based upon the density of the shale block, ρ_{shale}, the concentration of pyritic sulfur, $\%S_2$, and the concentration of calcium carbonate, $\%CaCO_3$.

$$\%FeS_2 = \%S_2 \cdot \frac{AM_{FeS2}}{AM_{S2}} \tag{3}$$

$$W_{FeS2} = \rho_{Shale} \cdot V_T \cdot \%FeS_2 \tag{4}$$

$$W_{CaCO_3} = \rho_{Shale} \cdot V_T \cdot \%CaCO_3 \tag{5}$$

Note that Eq 3 refers to AM_{FeS2}/AM_{S2}, which is the atomic mass ratio of pyrite to sulfide. Equation 6 describes the stoichiometry of pyrite oxidation that is required to determine the mass of sulfuric acid, W_{H2SO4}, and Eq 7 describes the stoichiometry of calcium carbonate reacting with sulfuric acid.

$$4FeS_2 + 15O_2 + 14H_2O = 4Fe(OH)_3 + 8H_2SO_4 \tag{6}$$

$$CaCO_3 + H_2SO_4 + 2H_2O = CaSO_4 2H_2O + CO_2 + H_2O \tag{7}$$

The stoichiometry of Eq 7 produces the required mass of calcium carbonate, WT_{CaCO3}, from the reaction with the sulfuric acid. There is a 2:1 $CaCO_3$:FeS_2 molar ratio required from Eq 7. If the amount of calcium carbonate available for the reaction, W_{CaCO3}, is less than the mass required to neutralize the sulfuric acid, WT_{CaCO3}, the gypsum volume calculation must be adjusted in accordance with Eq 8.

$$V_{Gypsum} = \frac{W_{Gypsum}}{\rho_{Gypsum}} \text{ if } W_{CaCO3} \geq WT_{CaCO3}$$
$$V_{Gypsum} = \left(\frac{W_{Gypsum}}{\rho_{Gypsum}} \cdot \frac{W_{CaCO3}}{WT_{CaCO3}}\right) \text{ if } W_{CaCO3} < WT_{CaCO3} \tag{8}$$

The mass of gypsum produced from Eq 7, W_{Gypsum}, is a function of the moles of gypsum produced and the atomic mass of gypsum. The density of gypsum, ρ_{Gypsum}, is approximately 2.3 g/cm^3.

FIG. 10

Pyritic shale expansion model. (*a*) Model assumes a block of pyritic shale with bedding or discontinuity planes perpendicular to uniformly and infinitely loaded surcharge area and in (*b*), (*c*), and (*d*) expansion of the shale block decreases as a function of the increase in void space and the decrease in elastic modulus. Note that the thickness of the gypsum infilling zones remains constant as the number of zones decrease as the amount of expansive material decreases.

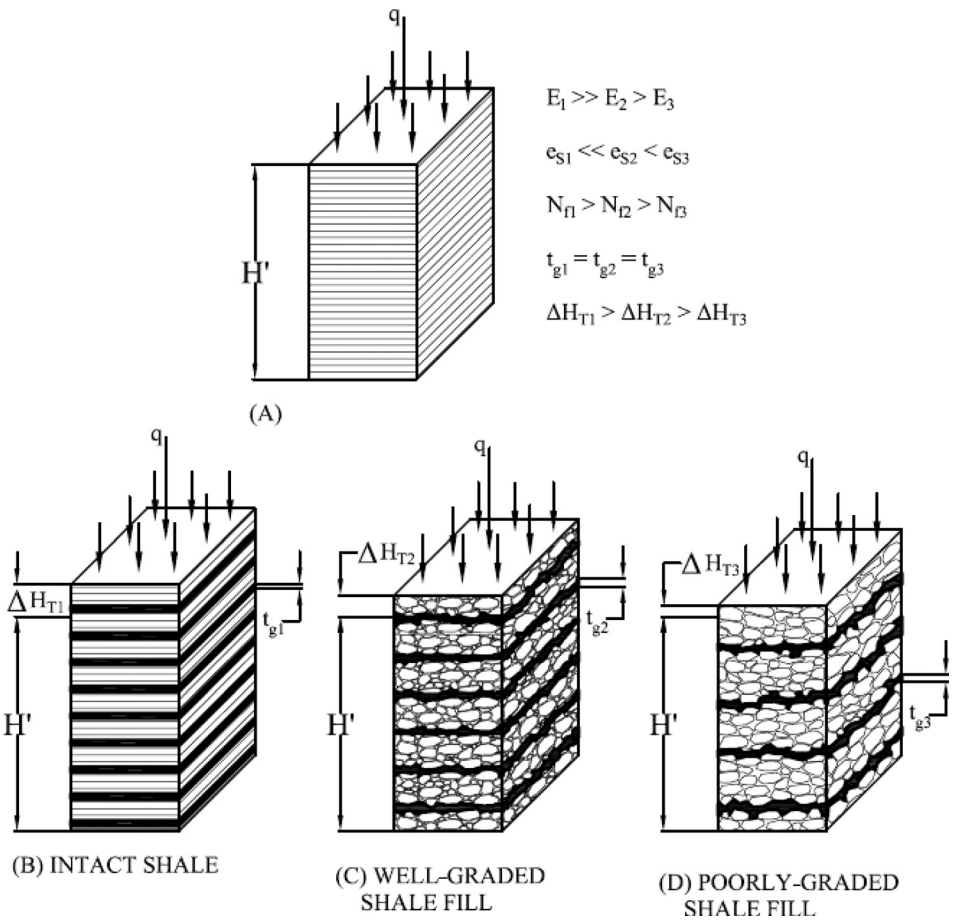

The expansion calculations are based on the gypsum infilling theory and are a direct function of the volume of gypsum determined from Eq 8. The volume of gypsum per discontinuity, V_{gf}, is a function of the assumed thickness of the gypsum infilling, t_g, and A_s and the number of gypsum fractures possible, N_f, is simply the total volume of gypsum from Eq 8, V_{Gypsum}, divided by the volume of gypsum per discontinuity, V_{gf}. Finally, the maximum theoretical expansion of the shale block, ΔH_G, is the product of number of fractures, N_f, and the thickness of the gypsum infilling, t_g. Equations 9, 10, and 11 describe the process that leads to maximum theoretical expansion, ΔH_G.

$$V_{gf} = t_g \cdot A_s \tag{9}$$

$$N_f = \frac{V_{\text{Gypsum}}}{V_{gf}} \tag{10}$$

$$\Delta H_G = N_f \cdot t_g \tag{11}$$

In order to account for the surcharge loading on the gypsum infilling and shale block, the elastic compression must be considered. Specifically, the elastic compression of the gypsum discontinuities is a function of the surcharge, q_t, the total thickness of the gypsum infilling, ΔH_G, the modulus of elasticity of gypsum, E_G, and Poisson's ratio of gypsum, υ_g. Equation 12 represents the elastic compression of the gypsum discontinuities, ΔH_{GE}.

$$\Delta H_{GE} = q_t \cdot \Delta H_G \cdot \frac{\left(1 - \upsilon_g^2\right)}{E_g} \tag{12}$$

The elastic compression of the shale block is also considered to fully understand the total compression resulting from expansion of the gypsum infilling and compression from the surcharge. The elastic compression of the shale block, E_{SE}, is represented by Eq 13 and is a function of the difference between the original height of the shale, H', and the thickness of the gypsum infilling, ΔH_G, the modulus of elasticity of the shale, E_S, and Poisson's ratio of shale, υ_s.

$$\Delta H_{SE} = q_t \cdot (H' - \Delta H_G) \cdot \frac{\left(1 - \upsilon_S^2\right)}{E_S} \tag{13}$$

The maximum total expansion, ΔH_G, including the elastic compression resulting from surcharge loading, is represented by Eq 14.

FIG. 11

Maximum swell potential graph showing normalized expansion (h/H) as a function of shale type, surcharge and pyritic sulfur content.

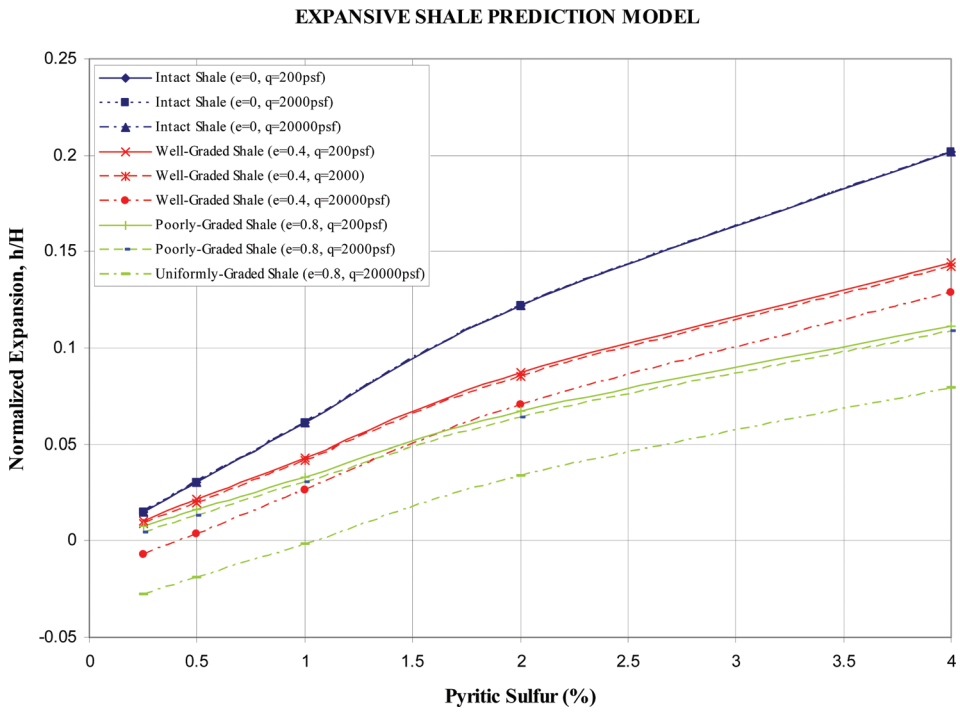

$$\Delta H_T = \Delta H_G - \Delta H_{GE} - \Delta H_{SE} \quad (14)$$

A correlation between the unconfined compressive strength and Young's modulus was developed by Arslan et al. (2007) for gypsum. This study determined an average gypsum modulus value of approximately 27 GPa (3916 ksi). Given the thickness and distribution of the gypsum infilling for this model, the value of the gypsum elastic compression at realistic loading values was determined to be insignificant ($\Delta H_{GE} \approx 0$); therefore, Eq 14 can be rewritten as follows:

$$\Delta H_T = \Delta H_G - \Delta H_{SE} \quad (15)$$

A number of typical input parameters were put into the model in order to see how the model compares to real world scenarios. Specifically, **Table 2** identifies the variable input parameters for the model trial.

Surcharge values for the model q_t were set at 9.577 kPa (200 lbf/ft^2), 95.77 kPa (2000 lbf/ft^2) and 957.7 kPa (20 000 lbf/ft^2) in order to determine the influence on the maximum expansion among the varying shale types. In addition, the pyritic sulfur concentration, $\%S_2$, was varied between 0.25 and 4.00 %. The thickness of gypsum infilling, t_g, was set at 0.05 cm (0.0196 in.) and the concentration of calcium carbonate, $\%CaCO_3$, was set at 10 %. The maximum swell potential model for these parameters is represented by **Fig. 11**.

As shown in **Fig. 11**, the model produces the greatest normalized expansion for the intact shale type and the surcharge amount has a negligible effect on the total expansion. The well-graded shale fill produces the next greatest amount of expansion with negligible expansion as a result of the increase of surcharge from 9.577 kPa (200 lbf/ft^2) to 95.77 kPa (2,000 lbf/ft^2) and 10 % decrease as the surcharge increases to 957.7 kPa (20,000 lbf/ft^2). The poorly-graded shale fill produces the least amount of expansion with negligible expansion as a result of the increase of surcharge from 9.577 kPa (200 lbf/ft^2) to 95.77 kPa (2000 lbf/ft^2) and 27 % decrease as the surcharge increases to 957.7 kPa (20 000 lbf/ft^2).

Note that the model produces a net negative amount of expansion for the well-graded shale at S_2 concentrations less than approximately 0.5 %, and for the poorly-graded shale at S_2 concentrations less than approximately 1.0 % at 957.7 kPa (20,000 lbf/ft2) surcharge.

Conclusions

The experimental trials presented in this paper reveal a number of interesting conclusions. Although geochemical testing did prove that pyritic oxidation did occur, the kinetic oxidation column experiment did not produce expansion on fresh/unweathered pyritic shale fragments. Expansion did occur in McCabe et al.'s (2012) passive expansion testing experiment; however, the shale samples were taken from a source where expansion had already begun. The hydrogen peroxide expansion testing model did produce expansion after an initial oxidation period

TABLE 3 Calculated maximum predicted total expansion and time to maximum expansion for experimental trials based on maximum theoretical expansion model.

Experimental Trial	Measured Rate (in./year/in.)	H (in.)	S_2 (%)	Maximum Normalized Expansion[b], h/H	Maximum Predicted Total Expansion[c], ΔH_G (in.)	Predicted Time to Maximum Expansion[d], t (years)
McCabe et al. maximum	0.0029	29.53	2.23[a]	0.070	2.07	24.1
McCabe et al. minimum	0.0023	39.37	2.23[a]	0.070	2.76	30.4
Sample A	0.0035	7.80	2.07	0.065	0.51	18.6
Sample D	0.0143	6.25	1.48	0.090	0.56	6.3

[a]Estimated average value from range of S_2 results from McCabe et al. 2012.
[b]h/H estimate expansion model (**Fig. 11**).
[c]$\Delta H_G = (h/H) \times H$.
[d]$t = (Rate)^{-1} \times (h/H)$.

on fresh/unweathered shale fragments. The experimental testing showed that once the oxidation and precipitation geochemical process starts, it proceeds on its own. McCabe et al. showed that a water source was not even necessary to continue the expansion process and the hydrogen peroxide experiment revealed the effectiveness in using a 10 % hydrogen peroxide solution to jump start the expansion process.

The theoretical expansion model is a simplistic attempt to quantify the maximum theoretical expansion of intact shale, well-graded shale fragments, and poorly-graded shale fragments. The model relies on the gypsum infilling theory and that all expansion takes place perpendicular to the surcharge loading. The theoretical model can be utilized to predict maximum expansion as well as the predicted time for maximum expansion to occur. **Table 3** presents calculations that reflect these predictions for the experimental trials presented.

The predicted total expansion results appear to be consistent with field measurements where heave of pyritic shales has resulted in structural damage (Bryant 2003). Predicted time to maximum expansion is more difficult to compare to field measurements since there is no known study that shows pyrite loss over time versus heave in either a pyritic shale fill or intact bedrock. Predicting total expansion and time from maximum expansion would allow engineers to make practical decisions regarding remediation to damaged structures. For example, engineers could determine if a structure could absorb additional movement or if more aggressive retrofitting would be in order.

Future research into expansive pyritic shales should focus on establishing a data base that will aid in refining the theoretical prediction models and providing guidance for standardized laboratory expansion and prediction procedures.

References

Anonymous, 1960, "Structures Don't Settle in this Shale, but Watch Out for Heave," *Eng. News Rec.*, Vol. 164, No. 5, pp. 46–48.

Brady, K. B. C., Smith, M. W., and Schueck, J., Eds., 1998, *Coal Mine Drainage Prediction and Pollution Prevention in Pennsylvania*, Pennsylvania Department of Environmental Protection, Harrisburg, PA.

Bryant, L. D., 2003, "Geotechnical Problems With Pyritic Rock and Soil," M.Sc. thesis, Virginia Polytechnic Institute and State University, Blacksburg, VA.

Coveney, R. M. and Parizek, E. J., 1977, "Deformation of Mine Floor by Sulfide Alteration," *Bull. Assoc. Eng. Geol.*, Vol. XIV, No. 1 pp. 131–156.

Dougherty, M. T. and Barsotti, N. J., 1972, "Structural Damage and Potentially Expansive Sulfide Minerals," *Bull. Assoc. Eng. Geol.*, Vol. IX, No. 2. pp. 105–125.

Dubbe, D. E., Usmen, M. A., and Moulten, L. K., 1984, "Expansive Pyritic Shales," *A Paper Offered for Publication by the Transportation Research Board*, Transportation Research Board, Washington, D.C.

Freeman, T. E., 2003, "Forensic Investigation of Pavement Distress: Old Airport Road in Bristol, Virginia," *Final Report*, Virginia Transportation Research Council, Charlottesville, VA.

Jangal, C. E., 1971, "Swelling Shale in the Ostersund Area," *Nat. Swed. Build. Res.*, Vol. R35, p. 116.

Jaynes, D. B., Pionke, H. B., and Rogowski, A. S., 1984a, "Acid Mine Drainage from Reclaimed Coal Strip Mines—2. Simulation Results of Model," *Water Resour. Res.*, Vol. 20, No. 2, pp. 243–250.

Jaynes, D. B., Rogowski, A. S., and Pionke, H. B., 1984b, "Acid Mine Drainage from Reclaimed Coal Strip Mines—1. Model Description," *Water Resour. Res.*, Vol. 20, No. 2, pp. 233–242.

Hawkins, A. B. and Pinches, G. M., 1987, "Cause and Significance of Heave at Llandough Hospital, Cardiff – A Case History of Ground Floor Heave Due to Gypsum Growth," *Q. J. Eng. Geol., Lond.* Vol. 20, No. 1, pp. 41–57.

Hoover, S. E., 2004, "Structural Damage Induced by Pyritic Shale," *Fifth International Conference on Case Histories in Geotechnical Engineering*, ISSMGE, New York, pp. 1–7.

Hoover, S. E. and Lehmann, D., 2009, "The Expansive Effects of Concentrated Pyritic Zones Within the Devonian Marcellus Shales Formation of North America," *Q. J. Eng. Geol. Hydrogeol.*, Vol. 42, No. 2, pp. 157–164.

Hoover, S. E. and Pease, J. B., 2007, "Micropile Underpinning Over Expansive Pyritic Shales," presented at the *8th International Workshop on Micropiles*, Toronto, Canada, Sept 26–30 (unpublished).

Long, J. D. and Williams, P. A., 1990, "Report of Structural Distress Investigation—Phase I, Johnson City Public Library," *S&ME*, Blountville, TN.

McCabe, B., Sutton, D., O'Connell, A., and Cripps, J., 2012, "A Laboratory Study of the Expansion of an Irish Pyritic Mudstone/Siltstone Fill Material," *Eng. Geol.* (under review).

Moum, J. and Rosenquist, I., 1959, "Sulfate Attack on Concrete in the Oslo Region," *J. Am. Concr. Inst.*, Vol. 56, pp. 257–264.

Penner, E. and Eden, W. J., 1972, "Expansion of Pyritic Shales," *Canadian Building Digest CBD-152*, National Research Council Canada, Windsor, ON.

Poole, A. B. and Thomas, A., 1975, "A Staining Technique for the Identification of Sulphates in Aggegrates and Concretes," *Miner. Mag.*, Vol. 40, 1975, pp. 315–316.

Rimstidt, J. D. and Newcomb, W. D., 1993, "Measurement and Analysis of Rate Data—The Rate of Reaction of Ferric Iron With Pyrite," *Geochim. Cosmochim. Acta*, Vol. 57, No. 9, pp. 1919–1934.

Schieber, J. and Baird, G., 2001, "On the Origin and Significance of Pyrite Spheres in Devonian Black Shales North America," *J. Sed. Res.*, Vol. 71, No. 1, pp. 155–166.

ACQC, 1999, *Pyrite and Your House*, Association Des Consommateurs Pour La Qualite Dans La Construction, Montreal.